The Clique Potential of Markov Random Field in a Random Experiment for Estimation of Noise Levels in 2D Brain MRI

Michael Osadebey,[1] Nizar Bouguila,[2]* Douglas Arnold,[3] The Alzheimer's Disease Neuroimaging Initiative

[1] Department of Electrical and Computer Engineering, Concordia University, Montreal, Quebec H3G 2W1, Canada

[2] Concordia Institute for Information Systems Engineering, Concordia University, Montreal, Quebec H3G 2W1, Canada

[3] NeuroRx Research Inc., 3575 Parc Avenue, Suite No. 5322, Montreal, Quebec H2X 4B3, Canada

Received 10 June 2013; accepted 22 August 2013

ABSTRACT: Effective performance of many image processing and image analysis algorithms is strongly dependent on accurate estimation of noise level. We exploit the simplicity and similarity of statistics of human anatomy among different subjects to develop new noise level estimation algorithm for magnetic resonance images of brain. Objects of the experiment are noise-free 3D brain MRI of 422 subjects. There are 21 slices for each subject. For each slice, total clique potential (TCP) of Markov random field, computed from local clique potential, is indexed by 200 different levels of noise. The sample space is the set of TCP-noise level data of each slice. The random variable is the set of indices of noise level of TCP in each element of sample space that is closest in numerical value to TCP measured from a test MRI slice. Noise level is estimated from the mean and variance of the random variable. We also report the formulation of a generalized mathematical model describing relationship between TCP and Rician noise level in brain MRI images. Our proposal can operate in the absence of signals in the background and significantly reduce modeling errors inherent in strong parametric assumptions adopted by some of the current algorithms. Int J Imaging Syst Technol, 23, 304–313, 2013; Published online in Wiley Online Library (wileyonlinelibrary.com). DOI: 10.1002/ima.22065

Key words: magnetic resonance imaging; single-layer Markov random field; total clique potential

I. INTRODUCTION

Noise level estimate in magnitude MRI images is required as input parameter for algorithms developed for the task of noise removal (Nowak, 1999; Basu et al., 2006; Wang and Zhou, 2006), segmentation (Zhang et al., 2001; Akselrod-Ballin et al. 2006), registration (Rohde et al., 2005), quality assessment of functional magnetic resonance images (Sendur et al.; 2005), overall quality assessment of magnetic resonance imaging systems (McVeigh et al., 1985; Tapiovaara and Wagner, 1993), and performance evaluation of noise removal algorithms (Milindkumar and Deshmukh, 2011).

We reviewed seven contributions (Henkelman, 1986; Brummer et al., 1993; Murphy et al., 1993; Chang et al., 2005; Sijbers et al., 2007; Aja-Fernandez et al., 2008; Rajan et al., 2010) in the literature on estimation of noise levels in brain MRI. Based on chronology, we

Correspondence to: Nizar Bouguila; e-mail: nizar.bouguila@concordia.ca
Data used in the design of the two algorithms proposed in this article were obtained from the Alzheimers Disease Neuroimaging Initiative (ADNI) database (adni.loni.ucla.edu). As such, the investigators within the ADNI provided data but did not participate in analysis or writing of this report. A complete listing of ADNI investigators can be found at: http://adni.loni.ucla.edu/wp-content/uploads/how_to_apply/ADNI_Acknowledgement_List.pdf. Accessed on September 21, 2013.

Grant sponsors: Data collection and sharing for this project was funded by the Alzheimer's Disease Neuroimaging Initiative (ADNI) (National Institutes of Health Grant U01 AG024904). ADNI is funded by the National Institute on Aging, the National Institute of Biomedical Imaging and Bioengineering, and through generous contributions from the following: Abbott; Alzheimer's Association; Alzheimer's Drug Discovery Foundation; Amorfix Life Sciences Ltd.; AstraZeneca; Bayer HealthCare; BioClinica, Inc.; Biogen Idec Inc.; Bristol-Myers Squibb Company; Eisai Inc.; Elan Pharmaceuticals Inc.; Eli Lilly and Company; F. Hoffmann-La Roche Ltd and its affiliated company Genentech, Inc.; GE Healthcare; Innogenetics, N.V.; IXICO Ltd.; Janssen Alzheimer Immunotherapy Research & Development, LLC.; Johnson & Johnson Pharmaceutical Research & Development LLC.; Medpace, Inc.; Merck & Co., Inc.; Meso Scale Diagnostics, LLC.; Novartis Pharmaceuticals Corporation; Pfizer Inc.; Servier; Synarc Inc.; and Takeda Pharmaceutical Company. The Canadian Institutes of Health Research is providing funds to support ADNI clinical sites in Canada. Private sector contributions are facilitated by the Foundation for the National Institutes of Health www.fnih.org. The grantee organization is the Northern California Institute for Research and Education, and the study is coordinated by the Alzheimer's Disease Cooperative Study at the University of California, San Diego. ADNI data are disseminated by the Laboratory for Neuro Imaging at the University of California, Los Angeles. This research was also supported by NIH grants P30 AG010129 and K01 AG030514.

classify them into two classes: the earlier and later groups. In the earliest, referred to as double acquisition method (Murphy et al., 1993), the same image is acquired twice, aligned, and subtracted. The noise level is estimated from the standard deviation of the subtracted image. Other early contributions (Henkelman, 1986; Brummer et al., 1993; Chang et al., 2005) estimate noise from the background region where the noise is described by Rayleigh distribution. The first later contribution (Sijbers et al., 2007) estimates noise level automatically from the maximum likelihood estimate of partial histogram of noise signal in the background region. The second in same category (Aja-Fernandez et al., 2008) estimates noise from local statistics in foreground where pixel intensities contaminated by noise are described by Gaussian distribution at high signal-to-noise-ratio and Rician at low signal-to-noise ratio. The third (Rajan et al., 2010) adopts maximum likelihood estimation principle to estimate the noise level from the local variance and local skewness of pixels.

The human brain is statistically simple and geometrically similar (Zhang et al., 2001; Osadebey, 2009). It is composed of only three major brain structures: white matter (WM), grey matter (GM), and the ventricular system (VS), each can be distinguished by its clearly defined range of voxel intensity values (Ashburner and Friston, 2003). Magnetic resonance imaging system reveals strong spatial, structural, and voxel statistical similarities among corresponding inter subject MRI slices. These similarity features are exploited in the design of single-subject MRI-based brain atlases (Evans et al., 1994; Mazziotta et al., 2001), which are widely acknowledged powerful tools in the analysis of brain images (Doan et al., 2010). We exploit this principle further by inferring that, across subjects, profiles describing variation of MRI slice voxel intensities with different levels of noise degradation will exhibit similar characteristics.

We regard each slice in a 3D MRI volume as similar "coin" or "dice" in a random experiment. Each "throw" or "roll" is the degradation of a noise-free MRI slice by 200 different levels of Rician noise. For each noise level, there is a corresponding outcome, the total clique potential of Markov random field. A slice is "thrown" 21 times (the number of slices in an individual subject's 3D MRI volume) and the experiment is repeated 422 times (total number of subjects). From the random experiment, we derive two separate sample spaces. The first is 2D of size $(422\times21=8862)\times200$. Each outcome of the sample space is TCP energy indexed by noise level for each slice. The second, derived from the mean of the first sample space, is 1D of size 1×200.

Our proposed algorithm is summarized in the schematic diagram displayed in Figure 1. Given a test image, TCP-noise level data is generated by degradation with increasing levels of noise, starting from zero noise level, up to $\sigma=200$. The data is normalized and the TCP zero variance energy is determined as the first element of the TCP-noise level data which corresponds to zero noise level. This prime energy value is numerically matched separately to each outcome in the two sample spaces resulting in two noise estimation results. The first noise estimate is determined from the mean and variance of the random variable generated from indices of each TCP-noise level data in the 2D sample space that is closest in numerical value to TCP-noise level data measured from the test image. The second noise level estimate is the unique index of MRF energy in the 1D sample space that is closest in numerical value to its counterpart in the test image data.

II. MATERIALS AND METHODS

A. Data for the Random Experiment. The objects of the random experiment were original, noise-free, 3 mm T_2 weighted axial 3D brain MRI sourced from the Alzheimer's Disease Neuroimaging Initiative (ADNI) database (www.adni.loni.ucla.edu). We chose as much as 422 subjects to satisfy the requirements of the central limit theorem (Leon-Garcia, 2008; Norman and Streiner, 2008; Walker and Shostak, 2010) and optimally extract similarities in the voxel statistics of inter subject brain MRI. The range, mean, and standard deviation of the subjects' age were 71–87, 75, and 10, respectively.

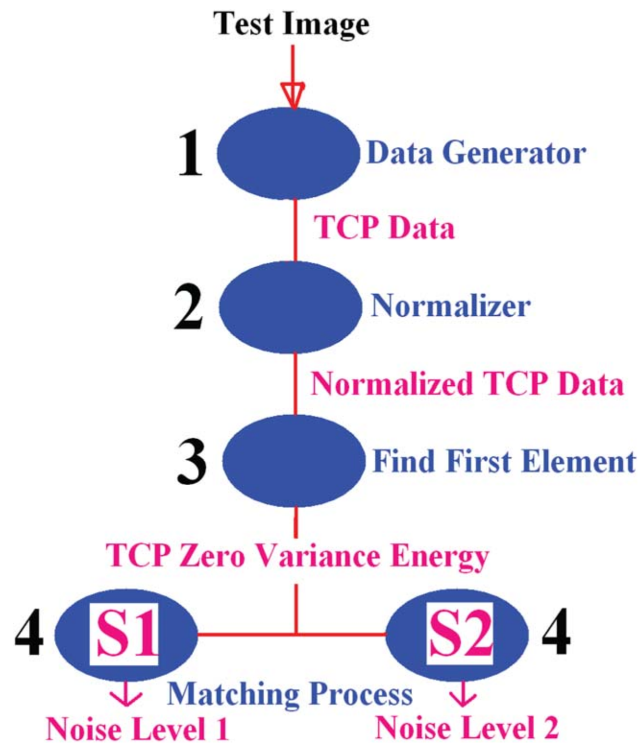

Figure 1. The four steps in the estimation of noise level in 2D brain MRI. In step 1, TCP-noise level data of the test image is generated. The data is normalized in step 2 and the first element (TCP zero variance energy) of the normalized data is extracted in step 3. In the estimation of the noise (step 4), the TCP zero variance energy is separately matched to each of the 1D and 2D sample spaces, S1 and S2, respectively. [Color figure can be viewed in the online issue, which is available at wileyonlinelibrary.com.]

ADNI was launched in 2003 by the National Institute on Aging (NIA), the National Institute of Biomedical Imaging and Bioengineering (NIBIB), the Food and Drug Administration (FDA), private pharmaceutical companies, and non-profit organizations, as 60 million dollars, 5-year public private partnership. The primary goal of ADNI has been to test whether serial magnetic resonance imaging (MRI), positron emission tomography (PET), other biological markers, and clinical and neuropsychological assessment can be combined to measure the progression of mild cognitive impairment (MCI) and early Alzheimer's disease (AD). Determination of sensitive and specific markers of very early AD progression is intended to aid researchers and clinicians to develop new treatments and monitor their effectiveness, as well as lessen the time and cost of clinical trials. The principal investigator of this initiative is Michael W. Weiner, MD, VA Medical Center and University of California in San Francisco. ADNI is the result of efforts of many co-investigators from a broad range of academic institutions and private corporations, and subjects have been recruited from over 50 sites across the US and Canada. The initial goal of ADNI was to recruit 800 adults (ages from 55 to 90) to participate in the research, approximately 200 cognitively normal older individuals to be followed for 3 years, 400

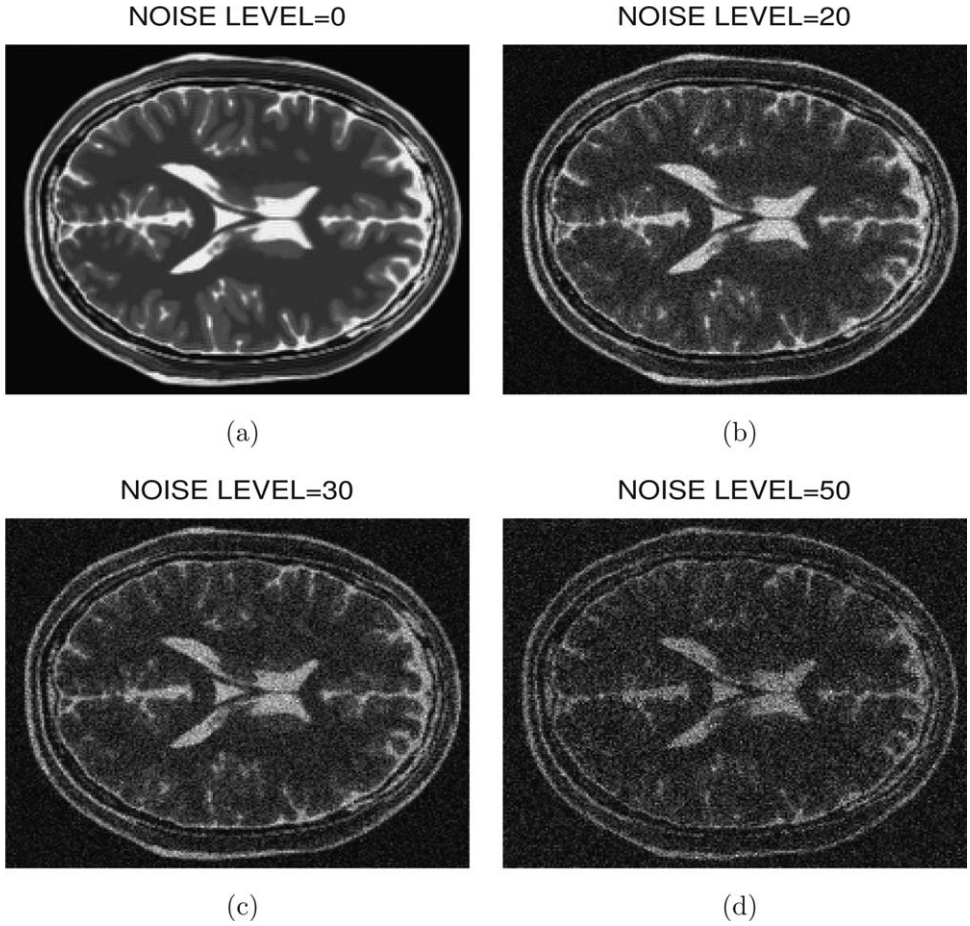

Figure 2. An MRI slice image at various levels of degradation by Rician noise (a) σ=0, (b) σ=20, (c) σ=30, and (d) σ=50.

people with MCI to be followed for 3 years, and 200 people with early AD to be followed for 2 years. For up-to-date information, the reader is referred to www.adni-info.org.

B. Single-Layered Markov Random Field. An image I is modeled as a single-layered Markov random field. Unlike the classical Markov random field theory (Geman and Geman, 1984), the observed image is the only physical system under consideration and there is no reference to a prior model. The Markov random field energy U is dependent on voxel configuration f. The voxel configuration is quantized into local cliques c in a clique system S that describes spatial coherence or clusters of similar voxels, so that the single-layered Markov random field energy is the sum of local clique potentials V_c:

$$U(f)=\sum_{c\in C} V_c(f) \tag{1}$$

For the clique system, we adopt second order neighborhood of size two with neighboring voxels indexed as (i,i'). In this system, the Markov random field energy is the sum of potential function contributions from single site and pair-site cliques (Li, 2009):

$$\hat{U}(f)=\sum_{i\in S}\alpha_1 V_1(f_i)+\sum_{i\in S}\sum_{i'\in N}\alpha_2 V_2(f_i,f_{i'}) \equiv E_a+E_b \tag{2}$$

where α_1, α_2 are interaction coefficients. The first term E_a referred to as the data term is the contribution from comparing each voxel intensity level to itself. The second term E_b, the smoothness term, is contribution from comparing each voxel intensity to its neighbors. At each local clique, the contribution of each neighboring voxel to the clique potential energy is determined according to the expression:

$$V_c(I(x,y))=\begin{cases}\xi_r & \mathbf{i}f\ I(i)=I_{(i')}\\ \xi_p & \mathbf{o}therwise\end{cases} \tag{3}$$

where ξ_r is the reward and ξ_p the penalty for conformity $(f_i=f_{i'})$ and violations $(f_i\neq f_{i'})$ of the smoothness constraints, respectively.

Noise changes the pattern of arrangement of pixels in the image as demonstrated in Figure 2. There is gradual change in pixel configurations for noise levels increasing from $\sigma=0$ in Figure 2a to $\sigma=20$, $\sigma=30$, and $\sigma=50$ in Figures 2b–2d, respectively. The different noise levels result in change in the strength of the clusters within the image. Thus, different noise levels σ give rise to different pixel configurations and their corresponding levels of energy $\hat{U}_\sigma(f)$. The data term is set to zero because it is a constant for different levels of noise. This renders the choice of values assigned to α_1 and α_2 in Eq. (2) irrelevant, hence for computational convenience, we set α_1 and α_2 to an arbitrary value of 1. For different image dimensions, we define total clique potential per pixel U:

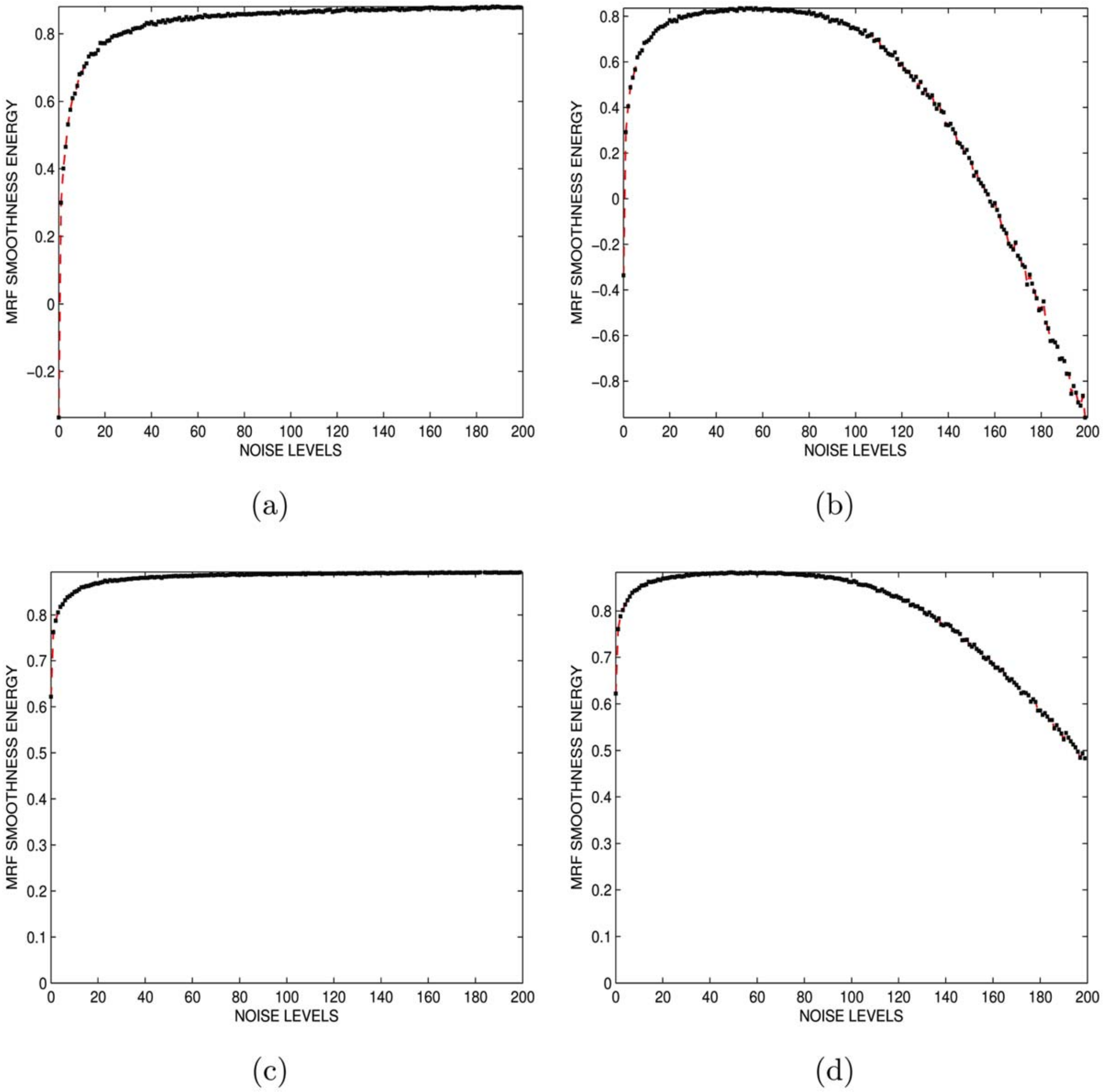

Figure 3. TCP energy-noise level curves associated with different image formats and combinations of conformity ξ_r and violations ξ_r of the smoothness constraints, (a) double precision and $(\xi_r=-8, \xi_p=1)$, (b) 8-bit integer and $(\xi_r=-8, \xi_p=1)$, (c) double precision and $(\xi_r=-1, \xi_p=1)$, and (d) 8-bit integer and $(\xi_r=-1, \xi_p=1)$. [Color figure can be viewed in the online issue, which is available at wileyonlinelibrary.com.]

$$U(f)=\frac{\hat{U}}{D}=\sum_{i\in S}\sum_{i'\in N}V_2(f_i,f_{i'}) \tag{4}$$

normalized by D, the product of row and column dimensions of the image.

It is well known that, in the presence of noise, the pixel intensities in the foreground of magnitude MRI follow a Rician distribution (Gravel et al., 2004):

$$P(M)=\frac{M}{\sigma^2}e^{-\frac{M^2+A^2}{2\sigma^2}}I_0\left(\frac{AM}{\sigma^2}\right)\varepsilon(M) \tag{5}$$

where A is the image pixel intensity in the absence of noise, M is the measured pixel intensity, I_0 is the modified zeroth order Bessel function of the first kind, and σ denotes the standard deviation of the Gaussian noise in the real and the imaginary images. In the background, where there is no image signal, the measured noise intensity is described by Rayleigh distribution.

$$P(M)=\frac{M}{\sigma^2}e^{-\frac{M^2}{2\sigma^2}} \tag{6}$$

With the exception of Murphy et al. (1993), most of current algorithms estimate noise from the probability distributions expressed in Eqs. (5) and (6). In our approach, we relate the potential function U expressed in Eq. (2) to the signal-to-noise ratio $(\frac{A}{\sigma^2})$, a variable on the right hand side of Eq. (5).

$$\sum_{i\in S}V_{1,\sigma}(f_i)+\sum_{i\in S}\sum_{i'\in N}V_{2,\sigma}(f_i,f_{i'})\equiv\left(\frac{A}{\sigma_n^2}\right) \tag{7}$$

It is noteworthy that the choice of ξ assigned to each clique is a strong determinant of the relationship between U and σ in Eq. (7). In

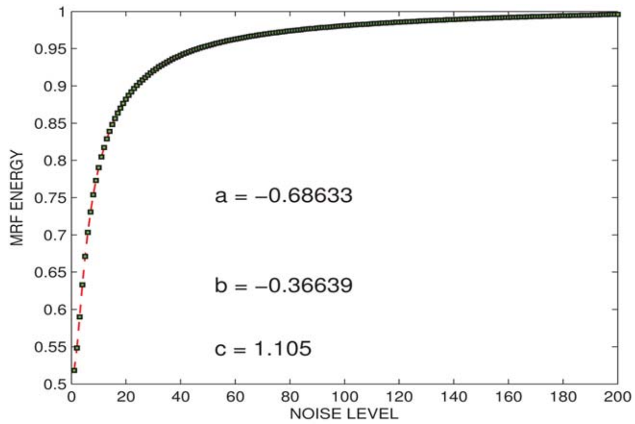

(a)

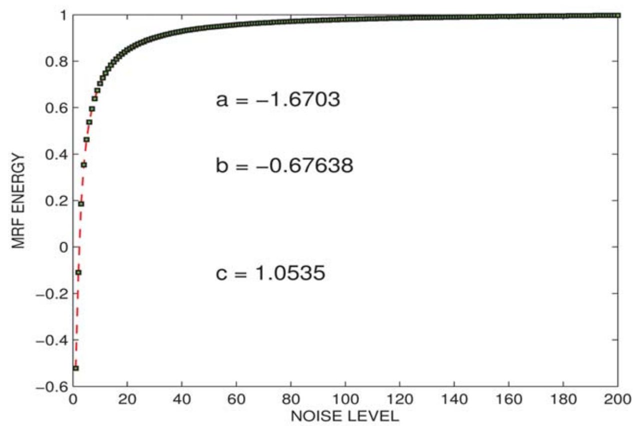

(b)

Figure 4. The plots of the proposed generalized mathematical models for describing the relationship between TCP energy and noise level in the (a) foreground and (b) background modes. [Color figure can be viewed in the online issue, which is available at wileyonlinelibrary.com.]

general, the relationship between the measured MRF energy of a MRI slice image and the noise levels can be expressed as:

$$U_{\sigma}(\xi,\chi,\sigma) \equiv (A\sigma_{\sigma}^{-2}) \tag{8}$$

where χ is the format of pixels in the image.

C. Simulation. The expression in Eq. (8) is under-constrained. To determine the model parameters, we made simulation of TCP energy-noise level relationship using images formatted as 8-bit unsigned integer and double precision, and for different values of cost assignments ξ_r, ξ_p for conformity and violations of the smoothness constraints, respectively. MRI Images (Figs. 3b and 3d) formatted as 8-bit unsigned integer generate data that can be modeled as quadratic form of polynomial function:

$$U(\sigma) \equiv \beta_k\sigma^k + \beta_{k-1}\sigma^{k-1} + \ldots + \beta_1\sigma + \beta_0 \tag{9}$$

where β is model parameter. They are ill-posed in the sense of Hadamard Bertero et al. (1988) because there is no unique MRF energy for all noise levels. Those that are double precision (Figs. 3a and 3c) are well-conditioned as they have unique values across the range of noise levels and can be described by power function:

$$U(\sigma) \equiv a\sigma^b + c \tag{10}$$

where a, b, c are model parameters. Based on the simulation results, MRI images most suitable for our algorithm are those with double precision and assignments $(\xi_r = -8, \xi_p = 1)$.

D. Sample Space. Let $W = 422$ be the number of noise-free 3D brain MRI data from different subjects. From each MRI data, $G = 21$ useful slices were extracted to obtain a total of $Z = GW$ slice images where each MRI slice image is indexed by $z \in [1, Z]$. Each MRI slice image indexed by z is replicated $L \in \mathbb{Z}$ number of times and each replica is further indexed by a replica number $l \in [1, L]$. Thus, each MRI slice image $I_{z,l}$ is indexed by its MRI slice number z in the database and its replica number l as defined by the set $\{(z,l) : 1 \le z \le Z, 1 \le l \le L\}$.

Starting from zero noise level, $\sigma=0$, each copy of MRI slice image is corrupted by increasing level of Rician noise $\{\sigma_l : \sigma_1, \sigma_2, \sigma_3, \ldots, \sigma_L\}$ weighted by the replica index. For each noise level of a replica image, the total clique potential energy (with and without background pixels) $U_{z,l}$ is computed from the sum of local clique potentials according to Eq. (4) to form a $1\times L$ TCP energy-noise level data $\{U_{z,l} : U_{z,1}, U_{z,2}, U_{z,3}, \ldots, U_{z,L}\}$. Each element of the TCP energy-noise level data is normalized by dividing it with the maximum value of the total clique potential in the TCP energy-noise level data so that $(-\infty \le U_{z,l} \le 1)$. For the entire MRI slices in the database, we obtain a 2D sample space Ω of normalized variations of TCP energy $U_{z,l}$ with noise level σ_l having dimensions $Z\times L$:

$$\Omega(\omega) = \begin{pmatrix} U_{1,1}, U_{1,2}, \ldots, U_{1,L} \\ U_{2,1}, U_{2,2}, \ldots, U_{2,L} \\ \ldots\ldots\ldots\ldots\ldots\ldots \\ \ldots\ldots\ldots\ldots\ldots\ldots \\ (U_{Z,1}, U_{Z,2}, \ldots, U_{Z,L} \end{pmatrix} \tag{11}$$

where each outcome ω of the sample space is each row of the matrix defined by $\omega = \{U_{z,l} : U_{z,1}, U_{z,2}, U_{z,3}, \ldots, U_{z,L}\}$. For notational convenience, we adopt same notations for normalized and unnormalized TCP data.

A second sample space κ having 1D of size $1\times L$ is derived from the 2D sample space by computing the mean of Eq. (11) along its column.

$$\kappa(l) = \frac{1}{Z}\sum_{z=1}^{Z} U_{z,l} \qquad \forall \quad l \tag{12}$$

Using regression analysis, we describe κ by a power model:

$$E = a\hat{\sigma}^b + c \tag{13}$$

$$a_b = -1.67, a_f = -0.6863 \tag{14}$$

$$b_b = -0.6764, b_f = -0.3663 \tag{15}$$

$$c_b = 1.053, c_f = 1.105 \tag{16}$$

where $a_b, a_f, b_b, b_f, c_b, c_f$ are the model parameters for the foreground (f) and background (b) modes. Plots of the power models are shown in Figure 4a for the foreground and Figure 4b for the background modes.

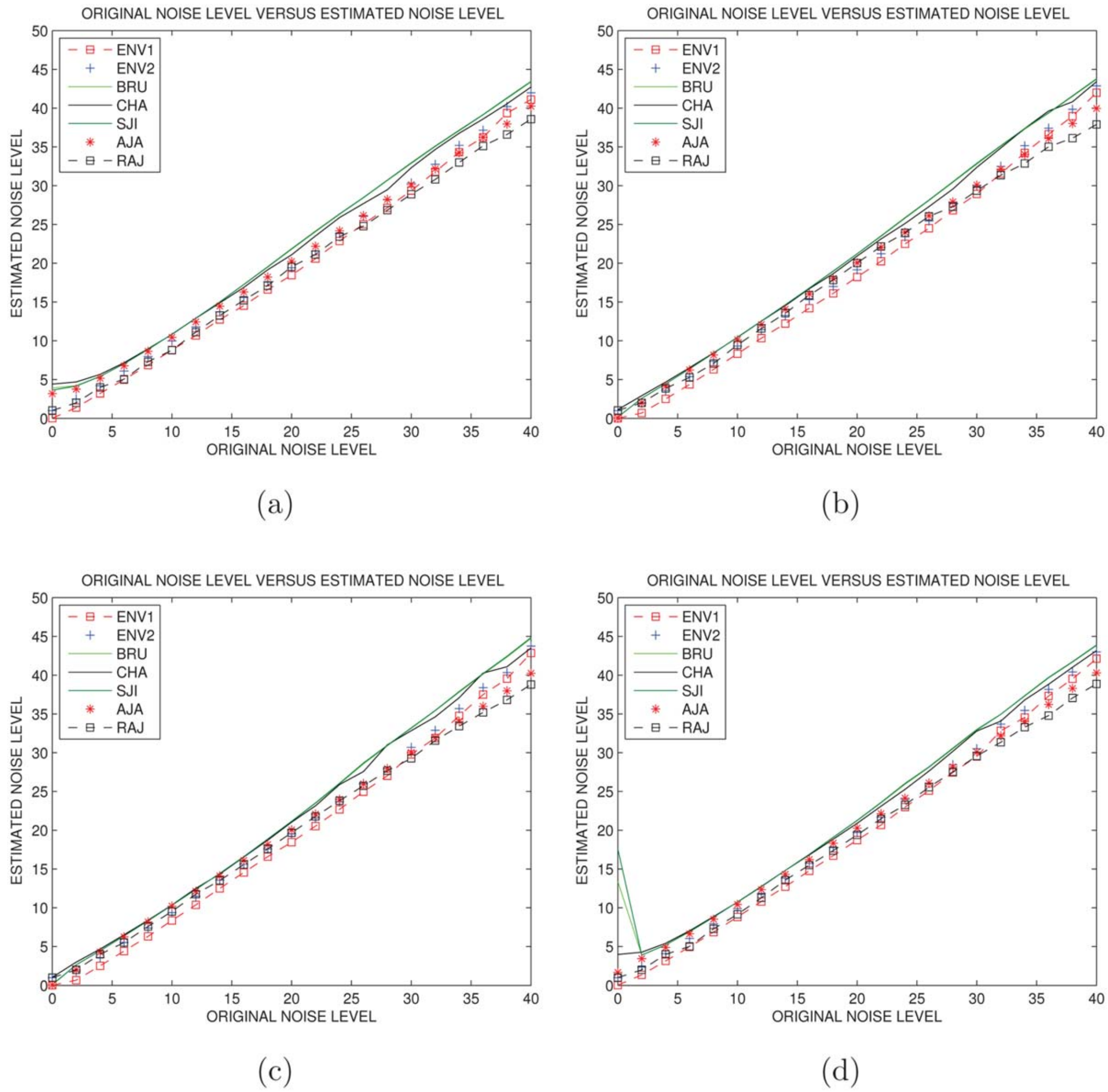

Figure 5. Comparative performance evaluation. The plots of the estimated noise levels $\hat{\sigma}$ versus original noise levels σ for four different MRI acquisitions: (a) T2, (b) T1, (c) PD, and (d) FLAIR. [Color figure can be viewed in the online issue, which is available at wileyonlinelibrary.com.]

E. Random Variable. A random variable X is defined as a function that assigns a real number $X(\omega)$, $\omega \in \Omega$, to each outcome ω in the sample space Ω of a random experiment (Leon-Garcia, 2008). Different random variables can be defined based on this random experiment. For example, there are a total of $T = ZL$ MRF energies indexed by $\{L : L < Z\}$ levels of noise. If Z is large enough such that $Z \gg L$, then T MRF energies will be randomly distributed into each noise level. Thus, the set of all possible MRF energies $\{\hat{U}_{1,l}, \hat{U}_{2,l}, \hat{U}_{3,l}, \cdots, \hat{U}_{Z,l}\}$, consisting of Z number of elements, that are indexed by a particular noise level l is a random variable. The random variable of interest to our proposal is defined as the set containing the indices $X_z(\omega)=\{l_1, l_2, l_3, \cdots, l_Z\}$, $l \in [1, L]$ of TCP energy $U_{z,l}$ in each outcome $\omega_z=\{U_{z,l} : 1 \leq z \leq Z, 1 \leq l \leq L\}$ of the sample space that is closest in value to the TCP energy measured from a test TCP image:

$$\{X_z(\omega)\}_{X_z \in [1,L]} = \arg\min_{l \in [1,L]} : \{l | \forall z : ||E_t - \{U_{z,l}\}||\} \tag{17}$$

F. Estimation of Noise Level. The test image is corrupted with increasing level $\{l : 0 \leq l \leq 200\}$ of Rician noise, starting from the first noise level $\sigma=0$. For each noise level, the TCP energy $E_{t,l}$ is computed according to Eq. (4) to obtain a 1×200 TCP energy-noise level data. The data is normalized by dividing each element with the maximum TCP energy. The normalized TCP energy $\hat{E}_{t,1}$ measured from the test image is the first element $l = 1$ of the normalized TCP energy-noise level data.

The normalized TCP energy measured from the test data is matched separately to each TCP energy-noise level data of an MRI slice in the 1D and 2D sample spaces. In both cases, we find the indices of the TCP energy in each TCP energy-noise level data that is closest in value to the normalized TCP energy measured from the test data.

The first matching generates random variable consisting of sequence of indices $X_z(\omega)=\{l_1, l_2, l_3, \cdots, l_Z\}$ of same number of elements Z as the MRI slice images in the sample space giving a total of Z number of Q unique discrete indices $\theta_z \in [0, L]$ each with

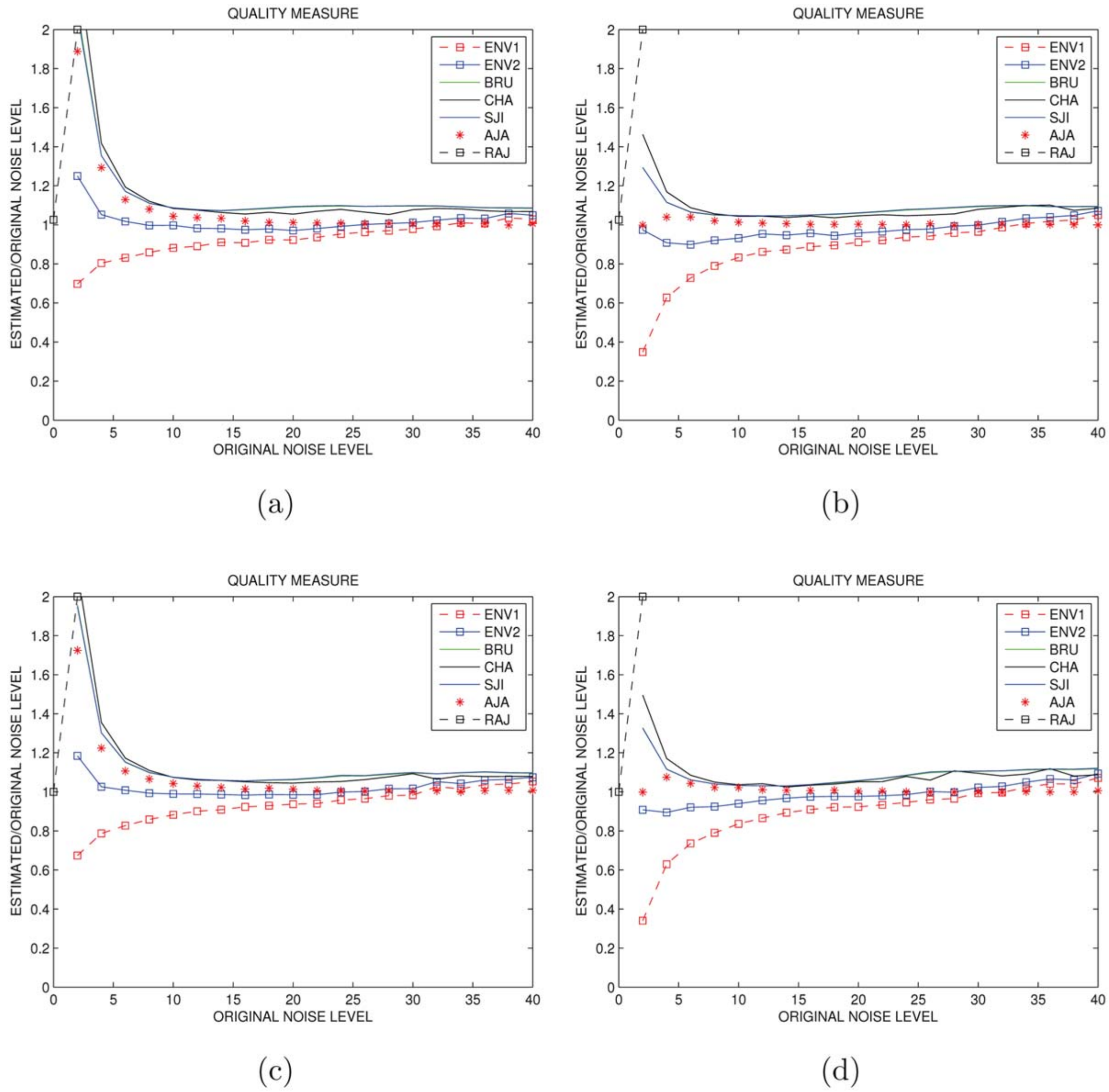

Figure 6. Comparative performance evaluation. The plots of the quality measures for four different MRI acquisitions: (a) T2, (b) T1, (c) PD, and (d) FLAIR. [Color figure can be viewed in the online issue, which is available at wileyonlinelibrary.com.]

frequency of occurrence λ_q. The estimated level of noise $ENV1$ is the mean of the probability distribution.

$$ENV1=\theta_1(\frac{\lambda_1}{Z})+\theta_2(\frac{\lambda_2}{Z})+\theta_3(\frac{\lambda_3}{Z})\ldots+\theta_Z(\frac{\lambda_Q}{D})-1 \tag{18}$$

The deviation from the mean is:

$$ENV1_{std}=\sqrt{\sum_{q=1}^{Q}(\theta_q-ENV1)^2\left(\frac{\lambda_q}{Z}\right)} \tag{19}$$

so that the estimate for the upper and lower limits of the noise level is $ENV1+ENV1_{std}$ and $ENV1-ENV1_{std}$, respectively.

The second matching generates only a single and unique index number $ENV2$ because the matching is with a single MRI energy-noise level data.

$$ENV2=\min_{l\in[1,L]}||\hat{E}_{t,1}-\kappa_l||-1 \tag{20}$$

The subtraction of unity in both Eqs. (18) and (20) is rescaling of the indices to account for index of noise level associated with Rician noise of zero variance.

The accuracy of the estimated noise level is strongly dependent on $\hat{E}_t$. To reduce error our algorithm monitors, the smoothness of the TCP energy-noise level data generated from the test image by computing its coefficient of variation $\{C_v|C_v\in\mathbf{Z}\}$, defined as the ratio of the standard deviation σ to its mean value μ, rounded to the nearest integer (Rosner, 2006).

$$C_v=\left(\frac{\sigma}{\mu}\right) \tag{21}$$

Based on trials of many test images, we set threshold value of $T_v=23$ for C_v. Below this threshold, the noise is estimated using the

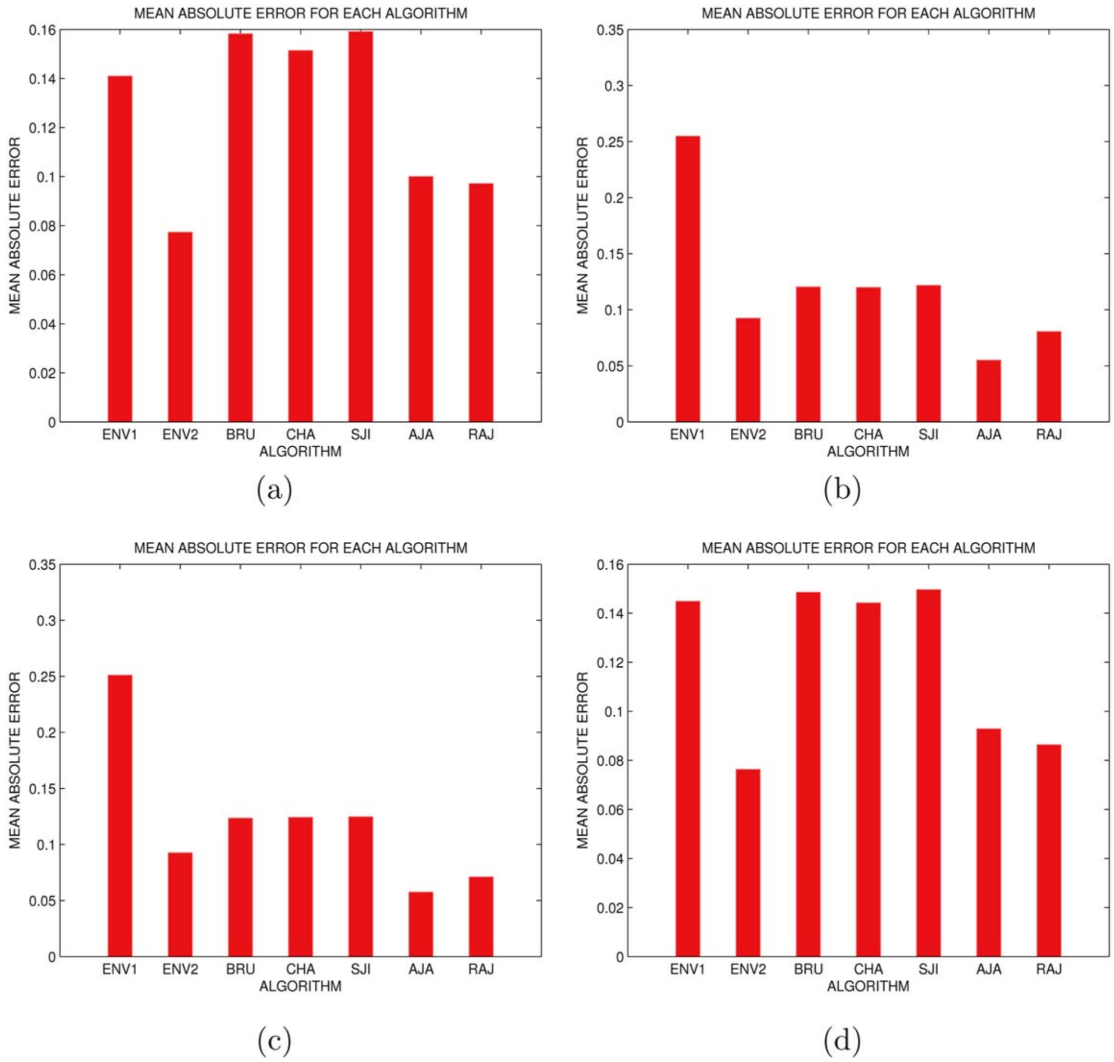

Figure 7. Comparative performance evaluation. The plots of the mean absolute error for four different MRI acquisitions: (a) T2, (b) T1, (c) PD, and (d) FLAIR. [Color figure can be viewed in the online issue, which is available at wileyonlinelibrary.com.]

first element $\hat{E}_{t,1}$ of the normalized test data as input parameter, and above it, the data is first fitted with a power model followed by updating $\hat{E}_t$ according to the following operation

$$E_{t,1} \rightarrow E_{t,N}, \qquad N=(T_v-C_v)\Delta \tag{22}$$

where N, an integer, is the index of the fitted model that is now assumed as the updated MRF energy computed from the test image and Δ is a user-defined correction factor, in the range $(0 \leq \Delta \leq 1)$, that takes into consideration the complexity of the features in the test image. In our case, we set $\Delta=1$ because each MRI slices of individual subjects in the database were free of noise and had undergone intensity correction.

III. RESULTS

A. Data for Evaluation. The test data are four different acquisition modes of real MRI data made available by NeuroRx research Inc., a Montreal based clinical research organization. They are T_1 relaxation time, T_2 relaxation time, and proton density (PD) as well as fluid attenuated inversion recovery (FLAIR). Each acquisition consists of thirty eight 3 mm axial MRI slices.

B. Comparative Performance Evaluation Results. The two methods of estimating noise in our proposed algorithm were denoted **ENV1** and **ENV2**. They were compared alongside five current algorithms. Brummer et al. (1993) **BRU**, Chang et al. (2005) **CHA**, Sijbers et al. 2007 **SJI**, Aja-Fernandez et al. (2008) **AJA**, and Rajan et al. (2010) **RAJ**. Each slice in the real MRI data was modified to follow Rician noise distribution ranging from $(0 \leq \sigma \leq 40)$. The artificially induced noise level was based on assumption that the magnitude MRI was acquired from real and imaginary data having equal standard deviations σ. For each original noise level σ, the estimate level of noise $\hat{\sigma}$ from an algorithm is determined from the mean value of noise level estimated for all individual slices in the volume data. The algorithms were compared based on four evaluation parameters. The plot of estimated noise level versus original noise level is displayed in Figure 5. The corresponding plots for quality measure, mean absolute error, and root mean square error are displayed in Figures 6–8, respectively.

IV. DISCUSSION

The algorithms were evaluated on images with both background and foreground signals. Three algorithms **BRU**, **CHA**, and **SJI**

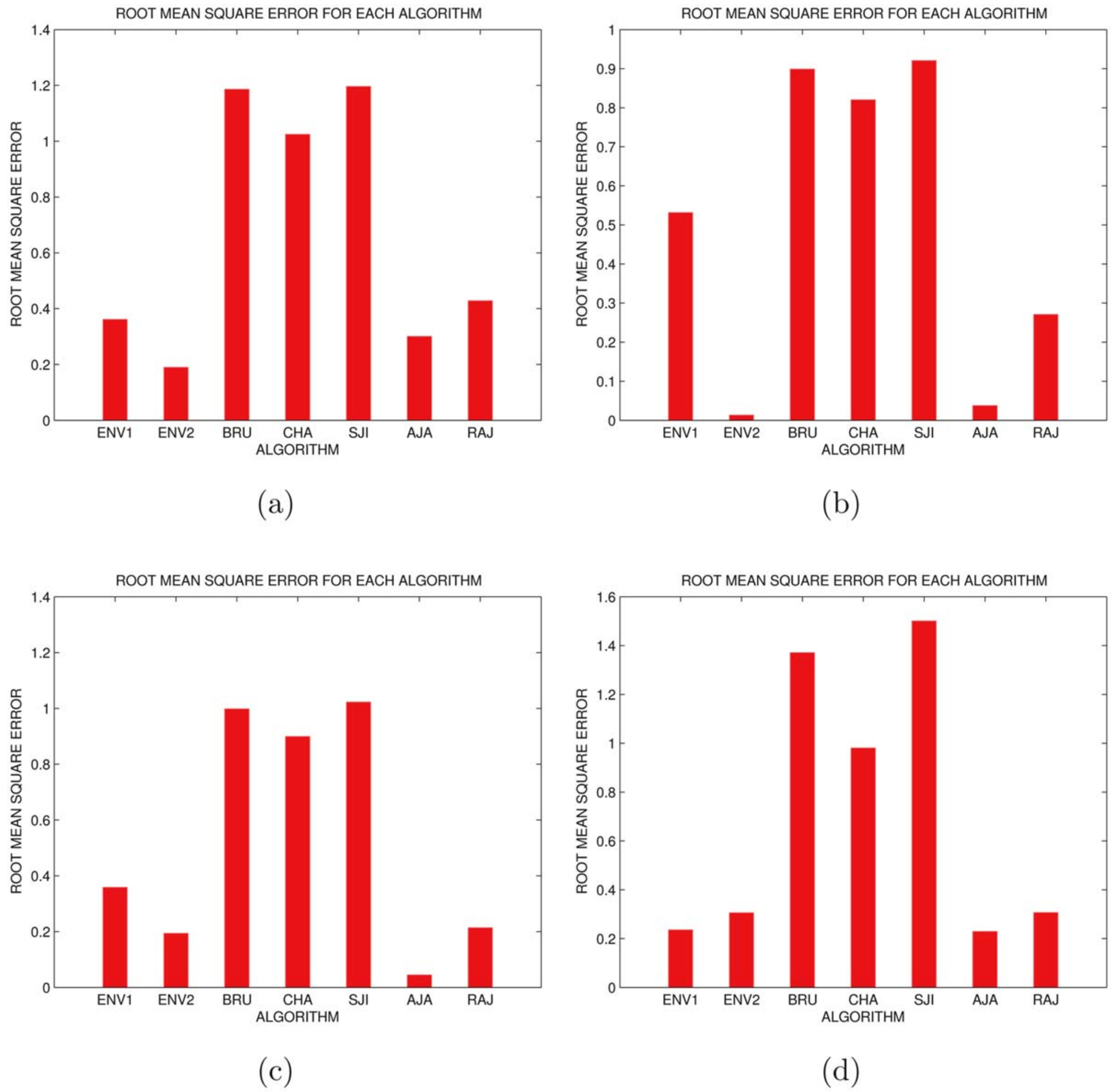

Figure 8. Comparative performance evaluation. The plots of the root mean square error for four different MRI acquisitions: (a) T2, (b) T1, (c) PD, and (d) FLAIR. [Color figure can be viewed in the online issue, which is available at wileyonlinelibrary.com.]

are designed to operate on images for which the background signal is clearly segmented from the foreground, and are therefore not optimal in performance in the presence of only foreground or limited background signals that are typical outputs of modern MRI scanners and MRI images with small field of view Rajan et al. (2010). Our proposal can be ranked alongside **AJA** and **RAJ** which can operate with and without background signals. Another state-of-the-art algorithm which can operate in the presence or absence of background was proposed by Coupe et al. (2010), but it is designed only for 3D MRI volume data. Our proposal can be adapted to measure noise level in 3D volume data by measuring noise level in each slice and averaging by the total number of slices in the volume. The time it takes to process an MRI slice is dependent on the mode adopted for estimation of noise level. On a computer having 3GB RAM and 1.65 GHz processor, the second approach **ENV2** can estimate noise level in an MRI slice in less than 10 s compared to **ENV1** that takes less than 30 s because it makes reference to a database.

The data points in the plots of estimated noise levels versus original noise levels in Figure 5 and quality measure in Figure 6 are strongly clustered at significant levels of noise. This indicates that all the algorithms under consideration are comparable to each other and that our proposal exhibit state-of-the-art characteristics of current algorithms. However, the distinction in their performances can be deduced from the plots of mean absolute errors and root mean square errors displayed in Figures 7 and 8, respectively.

The second approach in our proposal **ENV2** demonstrates superior performance in terms of mean absolute error (≈ 0.08) on T2 (Fig. 7a) and FLAIR (Fig. 7d) MRI images. In the same evaluation, parameter **AJA** was the best algorithm with (≈ 0.07) for T1 (Fig. 7b) and PD (Fig. 7c) images. It is closely followed by **RAJ** and our proposal **ENV2**.

Again our **ENV2** stands out clearly as the best algorithm based on root mean square error for T1 (Fig. 8b), (≈ 0.02) and T2 (Fig. 8a), (≈ 0.2) images. Closely behind is our first proposal **ENV1**, **AJA**, and **RAJ**. The algorithm **AJA** is the best for PD images

(≈ 0.2) closely followed by our two proposals **ENV1** and **ENV2** and **RAJ**. As can be seen in (Fig. 8d) for FLAIR images, the first approach in our proposal **ENV1** and **AJA** show the same level of best performance (≈ 0.2) and closely followed by our second proposal and **RAJ**.

V. CONCLUSION

We exploit the simplicity and similarity of statistics of human anatomy for different subjects in a random experiment and hereby propose a two-in-one application-specific algorithm that adopts the total clique potential of Markov random field energy as metric for estimation of noise variance in brain MRI. In the first approach, MRF energy is a variable in a random experiment. The second formulates the MRF energy-noise level relationship as a mathematical model. Both approaches are fast, accurate, and efficient in the estimation of noise variance. It is invariant to the presence or absence of background features in an image and is potentially immune to the modeling errors inherent in some of the current state-of-the-art algorithms.

ACKNOWLEDGMENTS

The source codes of other algorithms enabled us to carry out comparative performance evaluation of our algorithm. For this reason, we would like to express appreciation to the authors who provided their source codes. They are Dr. Santiago Aja-Fernandez and Jeny Rajan. We have special appreciation for Dr. Santiago Aja-Fernandez for implementing and making available to us the source codes of the work of authors in Brummer et al. (1993), Chang et al. (2005), and Sijbers et al. (2007). The Matlab source code of our proposed algorithm is available upon request. More experimental results and demo can be viewed at http://users.encs.concordia.ca/~m_osadeb/noise_estimation/results.htm.

REFERENCES

S. Aja-Fernandez, C. Alberola-Lopez, and C. Westin, Noise and signal estimation in magnitude MRI and Rician distributed images: A lmmse approach, IEEE Trans Image Process 17 (2008), 1383–1398.

A. Akselrod-Ballin, M. Galun, R. Basri, A. Brandt, M. Gomori, M. Filippi, and P. Valsasina, An integrated segmentation and classification approach applied to multiple sclerosis analysis, In: IEEE Computer Society Conference on Computer Vision and Pattern Recognition, 2006, pp. 1122–1129.

J. Ashburner and K. Friston, "Image segmentation," In Human Brain Function, R. Frackowiak, K. Friston, C. Frith, R. Dolan, K. Friston, C. Price, S. Zeki, J. Ashburner, and W. Penny (Editors), Academic Press, New York, 2003.

S. Basu, T. Fletcher, and R. Whitaker, Rician noise removal in diffusion tensor MRI, Proceedings of the 9th international conference on Medical Image Computing and Computer-Assisted Intervention (MICCAI'06), Vol. I (2006), pp. I17–125.

M. Bertero, T. Poggio, and V. Torre, Ill-posed problems in early vision, Proc IEEE 76 (1988), 869–889.

M. Brummer, R. Mersereau, R. Eisner, and R. Lewine, Automatic detection of brain contours in MRI data sets, IEEE Trans Med Imaging 12 (1993), 153–166.

L. Chang, G. Rohde, and C. Pierpaoli, An automatic method for estimating noise-induced signal variance in magnitude-reconstructed magnetic resonance images, Soc Photo-Opt Instrum Eng (SPIE) Conf Ser 5747 (2005), 1136–1142.

P. Coupe, J. Manjon, E. Gedamu, D. Arnold, M. Robles, and D. Collins, Robust Rician noise estimation for MR images, Med Image Anal 14 (2010), 483–493.

N. Doan, J.O. de Xivry, and B. Macq, Effect of inter-subject variation on the accuracy of atlas-based segmentation applied to human brain structures, Proc. SPIE, 2010, pp. 76231S–76231S–10.

A. Evans, M. Kamber, D. Collins, D. MacDonald, "An MRI-based probabilistic atlas of neuroanatomy," In Magnetic Resonance Scanning and Epilepsy, S. Shorvon, D. Fish, F. Andermann, G. Bydder, and H. Stefan, H. (Editors), Springer, New York, 1994, pp. 263–274.

S. Geman and D. Geman, Stochastic relaxation, Gibbs distributions, and the Bayesian restoration of images, IEEE Trans Pattern Recogn Mach Intell 6 (1984), 721–741.

P. Gravel, G. Beaudoin, and J.A.D. Guise, A method for modeling noise in medical images, IEEE Trans Med Imaging 23 (2004), 1221–1232.

R. Henkelman, Measurement of signal intensities in the presence of noise in MR images, Med Phys 12 (1986), 232–233.

A. Leon-Garcia, Probability, Statistics and Random Processes for Electrical Engineering, Prentice Hall, Upper Saddle River, NJ, 2008.

S. Li, Markov Random Field Modeling in Image Analysis, 3rd ed., Springer, New York, 2009.

J.C. Mazziotta, A.W. Toga, D.J. Evans, P. Fox, J. Lancaster, K. Zilles, R.P. Woods, T. Paus, G. Simpson, B. Pike, C. Holmes, L. Collins, P. Thomson, D. MacDonald, M. Iacoboni, T. Schormann, K. Amunts, N. Palomero-Gallagher, S. Geyer, L. Parsons, K. Narr, N. Kabani, G. Le Goualher, D. Boomsma, T. Cannon, R. Kawashima, and B. Mazoyer, A probabilistic atlas and reference system for the human brain: International Consortium for Brain Mapping (ICBM), Phil Trans R Soc Lond Ser B: Biol Sci 356 (2001), 1293–1322.

E.R. McVeigh, R.M. Henkelman, and M.J. Bronskill, Noise and filtration in magnetic resonance imaging, Med Phys 12 (1985), 586–591.

V. Milindkumar and P. Deshmukh, Performance evaluation of Rician noise reduction algorithm in magnetic resonance images, J Emerg Trends Comput Inf Sci 2 (2011), 39–44.

B. Murphy, P. Carson, J. Ellis, Y. Zhang, R. Hyde, and T. Chenevert, Signal-to-noise measures for magnetic resonance imagers, Magn Reson Imaging 11 (1993), 425–428.

G. Norman and D. Streiner, Biostatistics: The Bare Essentials, 3rd ed., People's Medical Publishing House, Shelton, CT, 2008.

R. Nowak, Wavelet based Rician noise removal for magnetic resonance images, IEEE Trans Image Process 8 (1999), 1408–1419.

M. Osadebey, Simulation of Realistic Head Geometry using Radial Vector Representation of Magnetic Resonance Image Data, Master's thesis, Tampere University of Technology, Finland, 2009.

J. Rajan, D. Poot, J. Juntu, and J. Sijbers, Noise measurement from magnitude MRI using local estimates of variance and skewness, Phys Med Biol 55 (2010), 441–449.

G. Rohde, A. Barnett, P. Basser, and C. Pierpaoli, Estimating intensity variance due to noise in registered images: Applications to diffusion tensor MRI, NeuroImage 26 (2005), 673–684.

B. Rosner, Fundamentals of Biostatistics, 6th ed., Cengage Learning Inc., Boston, MA, 2006.

L. Sendur, V. Maxim, B. Whitcher, and E. Bullmore, Multiple hypothesis mapping of functional MRI data in orthogonal and complex wavelet domains. IEEE Trans Signal Process 53 (2005), 3413–3426.

J. Sijbers, D. Poot, A. den Dekker, and W. Pintjens, Automatic estimation of the noise variance from the histogram of a magnetic resonance image, Phys Med Biol 52 (2007), 1335–1348.

M. Tapiovaara and R. Wagner, SNR and noise measurements for medical imaging: I. a practical approach based on statistical decision theory, Phys Med Biol 38 (1993), 71–92.

G. Walker and J. Shostak, Common Statistical Methods for Clinical Research with SAS Examples, 3rd ed., SAS Institute Inc., Cary, NC, 2010.

Y. Wang and H. Zhou, Total variation wavelet-based medical image denoising, Int J Biomed Imaging 2006 (2006), 1–28.

Y. Zhang, M. Brady, and S. Smith, Segmentation of brain MR images through a hidden Markov random field model and the expectation-maximization algorithm. IEEE Trans Med Imaging 20 (2001) 45–57.